

DIRECTLY DETERMINED LINEAR RADII AND EFFECTIVE TEMPERATURES OF EXOPLANET HOST STARS

GERARD T. VAN BELLE¹ AND KASPAR VON BRAUN²

Submitted to ApJ on 15.10.2008, accepted on 27.12.2008

ABSTRACT

We present interferometric angular sizes for 12 stars with known planetary companions, for comparison with 28 additional main-sequence stars not known to host planets. For all objects we estimate bolometric fluxes and reddenings through spectral energy distribution fits, and in conjunction with the angular sizes, measurements of effective temperature. The angular sizes of these stars are sufficiently small that the fundamental resolution limits of our primary instrument, the Palomar Testbed Interferometer, are investigated at the sub-milliarcsecond level and empirically established based upon known performance limits. We demonstrate that the effective temperature scale as a function of dereddened $(V - K)_0$ color is statistically identical for stars with and without planets. A useful byproduct of this investigation is a direct calibration of the T_{EFF} scale for solar-like stars, as a function of both spectral type and $(V - K)_0$ color, with an precision of $\overline{\Delta T}_{(V-K)_0} = 138\text{K}$ over the range $(V - K)_0 = 0.0 - 4.0$ and $\overline{\Delta T}_{\text{SpType}} = 105\text{K}$ for the range F6V - G5V. Additionally, we provide in an appendix spectral energy distribution fits for the 166 stars with known planets which have sufficient photometry available in the literature for such fits; this derived “XO-Rad” database includes homogenous estimates of bolometric flux, reddening, and angular size.

Subject headings: infrared: stars, stars: fundamental parameters, techniques: interferometric

1. INTRODUCTION

The formation, evolution, and environment of extrasolar planets are heavily influenced by their respective parent stars, including the location and extent of the habitable zone. To provide constraints on the characterization of these planets, it is therefore of significant scientific value to directly determine the astrophysical parameters of the host stars. Of particular interest are stellar radius (R) and effective surface temperature (T_{EFF}) since these two parameters help uniquely characterize our knowledge of extrasolar planet environments. In the case of radius, planetary radii are frequently not directly measured but established through observations of transit events as a ratio of planet to stellar radius. Measurements of planetary temperature are directly linked to the spectral characteristics of the star irradiating the planet.

For extrasolar planet hosting stars (EHSs) that can be resolved with interferometers, their angular sizes (θ) are directly measured. Since the Stefan-Boltzman Law (Stefan 1879; Boltzmann 1884) can be rewritten as $T_{\text{EFF}} \sim (F_{\text{BOL}}/\theta^2)^{1/4}$, where F_{BOL} is the reddening-corrected bolometric flux, the effective temperature T_{EFF} can be directly measured for these stars. We obtained data with the Palomar Testbed Interferometer (PTI) for 9 nearby EHSs with the aim of directly measuring their angular diameters, and computed estimates of their F_{BOL} through spectral energy distribution (SED) fitting to their available literature photometry. Additional EHS angular diameters from the Center for High Angular Resolution Astronomy (CHARA) Array are also folded into

this investigation (Baines et al. 2007, 2008a). Further interferometric work relevant to the diameters of EHSs can be found in Mozurkewich et al. (1991, 2003).

Observational biases cause a large fraction of known EHSs to be nearby, enabling the use of Hipparcos parallaxes for a direct determination of their distances (Perryman et al. 1997; Perryman & ESA 1997); in combination with angular size measurements, their linear radii can be determined.³

The aim of this publication is to provide directly determined R and T_{EFF} astrophysical parameters of these 12 EHSs along with equivalently derived parameters for a control group of 28 main sequence stars not currently known to host extrasolar planets. In addition, we present estimates of astrophysical parameters for all currently known EHSs with sufficient literature photometry (166 of the 230 known)⁴. The literature photometry and aforementioned SED fitting provides, for the sample of 166 EHS stars, estimates of F_{BOL} and θ_{EST} , done in the same way as done by van Belle et al. (2008), if a T_{EFF} is assumed to be associated with the particular SED template being used to fit the stellar photometry. These estimates of F_{BOL} and θ_{EST} are presented in the “XO-Rad” database at the end of this paper.

We describe the observations and data reduction of

³ It is misleading, however, to indicate that interferometric angular size measurements independently lead to characterizations of stellar luminosity. A *common mistake* is to assume that radius and temperature measurements derived from a single interferometric angular size can be combined through use of the Stefan-Boltzman law ($L \sim R^2 T_{\text{EFF}}^4$) to ‘measure’ luminosity. A cursory examination of the relationship between angular size and radius ($R \sim \theta$) and temperature ($T_{\text{EFF}} \sim \theta^{-1/2}$) will demonstrate the new information contained in an angular size measurement is discarded when calculating L : only bolometric flux and distance information affect measures of L .

⁴ As of Feb. 1, 2008.

¹ European Southern Observatory, Karl-Schwarzschild-Str. 2, 85748 Garching; gerard.van.belle@eso.org

² NASA Exoplanet Science Institute, California Institute of Technology, MC 100-22, Pasadena, CA 91125; kaspar@ipac.caltech.edu

these stars in §4; supporting data and spectral energy distribution fits are described in §3; derived effective temperatures and radii are presented in §5, along with comparisons of our values to previous investigations (where available); finally, a detailed statical comparison of the EHS stars versus our control group is seen in §5.3.

2. DESCRIPTION OF THE DATASETS

We present interferometric results on two different datasets:

1. Known EHSs for which we were able to obtain PTI data (§4) and calculate angular radii (§5). Knowledge of angular radii imposes an independent constraint on the SED fitting (§3) and allows T_{EFF} to be determined directly. We were also able to augment our PTI data with 7 stars published from the CHARA Array by Baines et al. (2008a). This dataset comprises 12 stars, 4 of which have data from both CHARA and PTI. Together this sample of EHSs with angular sizes is our ‘EHSA’ sample.
2. A number of main-sequence stars for which it was deemed possible to resolve angular radii using PTI. This dataset comprises 28 stars and will be referred to as our ‘control sample’. These stars are not currently known to host extrasolar planets and thus serve as a comparison group for the EHSs with respect to astrophysical parameters.

Additionally, SED fits are provided for all the well-characterized EHSs (status 1 Feb 2008, according to the Exoplanet Encyclopedia⁵). The source dataset comprises approximately 230 stars (including the ones for which we obtained PTI data), although most of the fainter ($V > 10$) stars are excluded due to a lack of available photometry; they are presented in the “X0-Rad” database in Appendix A. SED fitting for these stars is performed based on literature photometry and spectral templates with associated estimates of effective temperatures.

3. SUPPORTING DATA AND SPECTRAL ENERGY DISTRIBUTION FITTING

For all of the sources considered in this investigation, spectral energy distribution (SED) fits were performed. Each fit, accomplished using available photometry and an appropriate template spectrum, produces estimates for the bolometric flux (F_{BOL}), the angular diameter (θ_{EST}) and the reddening (A_V); effective temperature during the SED fit is fixed for each of the template spectra. In the absence of direct measurement of the angular diameter (i.e. calibrators and stars listed in the X0-Rad database), SED fitting is used to estimate the angular size. When the angular diameter is available from interferometric measurements, SED fitting is used to determine the bolometric flux and the reddening; effective temperature as well as dereddened colors can then be derived.

These SED fits are accomplished using photometry available in the literature as the input values, with template spectra from the Pickles (1998) library appropriate for the spectral types indicated for the stars in question.

Spectral types used in the SED fitting for all EHS stars are those values found in the Exoplanet Encyclopedia, which is in turn based upon the respective source discovery papers cataloged therein. The control sample stars as defined in §2 had their spectral types established from those values found in Hipparcos catalog (Perryman et al. 1997).

The template spectra are adjusted by the fitting routine to account for overall flux level, wavelength-dependent reddening, and expected angular size. Reddening corrections are based upon the empirical reddening determination described by Cardelli et al. (1989), which differs little from van de Hulst’s theoretical reddening curve number 15 (Johnson 1968; Dyck et al. 1996). Both narrowband and wideband photometry in the $0.3 \mu\text{m}$ to $30 \mu\text{m}$ are used as available, including Johnson UBV (see, for example, Eggen 1963; Moreno 1971) Stromgren $ubvy\beta$ (Piirola 1976), 2MASS JHK_s (Cutri et al. 2003), Geneva (Rufener 1976), and Vilnius $UPXYZS$ (Zdanavicius et al. 1972); flux calibrations are based upon the values given in Fukugita et al. (1995) and Cox (2000). The results of the fitting for the calibrator stars is given in Table 1; for the EHSA and control sample stars, Table 6, and for the “X0-Rad” database, Table 7.

4. OBSERVATIONS AND DATA REDUCTION

4.1. Visibility and Angular Sizes

The calibration of the target star visibility (V^2) data is performed by estimating the interferometer system visibility (V_{SYS}^2) using the calibration sources with model angular diameters and then normalizing the raw target star visibility by V_{SYS}^2 to estimate the V^2 measured by an ideal interferometer at that epoch (Mozurkewich et al. 1991; Boden et al. 1998; van Belle & van Belle 2005). Uncertainties in the system visibility and the calibrated target visibility are inferred from internal scatter among the data in an observation using standard error-propagation calculations (Boden et al. 1999). Calibrating our point-like calibration objects against each other produced no evidence of systematics, with all objects delivering reduced $V^2 = 1$.

Visibility and uniform disk angular size (θ_{UD}) are related using the first Bessel function (J_1): $V^2 = [2J_1(x)/x]^2$, where spatial frequency $x = \pi B \theta_{\text{UD}} \lambda^{-1}$. We may establish uniform disk angular sizes for the target stars observed by the interferometer since the accompanying parameters (projected telescope-to-telescope separation, or baseline, B and wavelength of observation λ) are well-characterized during the observation. The uniform disk angular size can (and should) be connected to a more physical limb darkened angular size (θ_{LD}); however, this is a minor effect since $\theta_{\text{LD}}/\theta_{\text{UD}}$ is small in the near-infrared ($< 1.5\%$; see, for example, Scholz & Takeda 1987; Tuthill 1994; Dyck et al. 1996, 1998; Davis et al. 2000).

Strictly speaking, limb darkened angular size is utilized here as a reasonable proxy for the Rosseland angular diameter, which corresponds to the surface where the Rosseland mean optical depth equals unity, as advocated by Scholz & Takeda (1987) as the most appropriate surface for computing an effective temperature. The dense, compact atmospheres of the stars considered in this in-

⁵ <http://exoplanet.eu/>

vestigation are well characterized by a uniform disk fit, and the small correction factors tabulated in Davis et al. (2000) will be used to convert our θ_{UD} sizes into the appropriate limb darkened θ_{LD} numbers. The number of visibility points $N(V^2)$, derived θ_{UD} sizes, associated goodness-of-fit χ^2_ν and residuals (δV^2), Davis et al. (2000) correction factors $\theta_{\text{LD}}/\theta_{\text{UD}}$ and resultant θ_{LD} sizes are found in the first columns of Table 6.

4.2. PTI Observations

PTI is an 85 to 110 m *H*- and *K*-band 1.6 μm and 2.2 μm interferometer located at Palomar Observatory in San Diego County, California, and is described in detail in Colavita (1999). It has three 40-cm apertures used in pairwise combination for detection of stellar fringe visibility on sources that range in angular size up to 5.0 milliarcseconds (mas), being able to resolve individual sources with angular diameter (θ) greater than 0.60 mas in size. PTI has been in nightly operation since 1997, with minimum downtime throughout the intervening years. The data from PTI considered herein cover the range from the beginning of 1998 (when the standardized data collection and pipeline reduction went into place) until the beginning of 2008 (when the analysis of this manuscript was begun). In addition to the target stars discussed herein, appropriate calibration sources were observed as well and can be found *en masse* in van Belle et al. (2008). Additional calibration sources of minimal angular size, as discussed in §4.3, were also selected and are listed in Table 1.

4.3. Limits of PTI Calibration

As discussed by Boden et al. (1998, 1999), PTI has an empirically established fundamental limiting visibility measurement error of $\sigma_{V^2_{\text{SYS}}} \approx 1.5\%$. The source of this limiting night-to-night measurement error is most likely a combination of effects: uncharacterized atmospheric seeing (in particular, scintillation), detector noise, and other instrumental effects.

This night-to-night repeatability limit restricts the ultimate resolution of the instrument. This is at odds with the desire to measure stellar diameters which, for a given brightness, are quite small in an angular sense relative to PTI's resolution. Main sequence stars are squarely in this regime for PTI, with only a few examples - those considered in this investigation - that creep out of the nether regions of point-like obscurity into the realm of resolvability. Attempting to resolve stars at the edge of PTI's performance envelope requires careful consideration of the demonstrated limits of the instrument, using the techniques described in van Belle & van Belle (2005, henceforth Paper VB2).

For PTI, operating at the *K*-band with its 109-m N-S baseline, a target of 0.60 milliarcseconds (mas) in size should have a normalized visibility of $V^2 = 94.89\%$ (as introduced in §4.1). As discussed in VB2, there is a strong motivation towards using calibration sources that are as point-like as possible - generally speaking, one wishes to have calibration sources that are significantly smaller than the targets being observed. For this investigation, to reach the regime of 0.60 mas targets, we restricted our use of calibrators to those that are, on average, 0.35 mas or less in size. These two size limits are

selected to have sufficient numbers of sufficiently bright targets and calibrators, respectively.

For such calibrators, observed by PTI, the visibility calibration limit is $\sigma_{V^2} = 0.186\%$ (from VB2, Equation 7), which contributes an angular size error due to calibration of roughly 0.012 mas. The night-to-night limiting V^2 measurement error of $\sigma_{V^2_{\text{SYS}}} \approx 1.5\%$, however, contributes an angular size error of 0.086 mas. This is significant in that the measurement error dominates any possible calibration bias, which is particularly important when considering smaller targets. If we were instead to have selected calibrators closer to ~ 0.70 mas in size - more typical of PTI investigations that observe larger targets that are > 1 mas in size - then the calibration angular size error be ~ 0.045 mas, and would start to compete with the measurement error in dominating the error budget. This would put our results at substantial risk of directly reporting any measurement bias inherent in the process we used to estimate the angular sizes of our calibration sources. Since our goal is direct measurement of the target angular sizes, we have taken great care to ensure that this is not the case.

A second aspect of this consideration of PTI limiting performance is the reported angular sizes of our target stars. For stars that, after calibration, report formal errors that are sufficiently small to be in violation of PTI's known night-to-night repeatability, we increased their reported angular size errors to the level consistent with that repeatability. As a function of target angular size, we show the limits of angular size accuracy possible with PTI's repeatability limit in Table 2. The first column shows various target angular sizes, followed by the corresponding visibilities. A calibrator of 0.35 mas, as noted above, contributes a the limit on knowledge of visibility of $\sigma_{V^2} = 0.186\%$; the associated limit in angular size knowledge is then listed in column three. The next two columns list the night-to-night repeatability limit of V^2 , and the associated angular size error. The final column combines the calibration limit and the night-to-night limit in quadrature.

4.4. CHARA EHS Data

Additional angular diameters of EHSs were obtained with the Georgia State University CHARA Array (Baines et al. 2008a) with an intent of detecting possible face-on binarity masquerading as planetary companionship (Baines et al. 2008b). The CHARA Array is a optical/near-infrared interferometer similar to PTI (ten Brummelaar et al. 2005), but with longer baselines (up to 330m), allowing for resolution of smaller objects. For inclusion of the appropriate CHARA data into our dataset, we will apply observation criteria similar to the PTI data: First, the calibration sources must be sufficiently unresolved, which we set for CHARA to be 0.50mas or less. Second, the ratio of angular sizes of science targets and their calibrators must be greater than 1.5. In applying these two criteria, we are confident that the resulting measured angular sizes are sufficiently independent of the calibrator angular sizes predicted by SED fitting.

The resulting dataset for inclusion in this analysis consists of seven EHS angular sizes from the CHARA investigation, of which four stars are common to both the

TABLE 2
 CALIBRATION FLOOR BY TARGET ANGULAR SIZE AS DISCUSSED IN §4.3.

Target θ (mas)	Target V^2	Calibration σ_{V^2}	Calibration σ_θ (mas)	Night-to-night σ_{V^2}	Night-to-night σ_θ (mas)	σ_θ floor (mas)
0.600	0.94893	0.00186	0.012	0.01500	0.085	0.086
0.650	0.94028	0.00186	0.010	0.01500	0.079	0.080
0.700	0.93103	0.00186	0.010	0.01500	0.075	0.076
0.750	0.92116	0.00186	0.010	0.01500	0.071	0.072
0.800	0.91072	0.00186	0.009	0.01500	0.068	0.069
0.850	0.89971	0.00186	0.008	0.01500	0.064	0.065
0.900	0.88815	0.00186	0.008	0.01500	0.062	0.063
0.950	0.87607	0.00186	0.008	0.01500	0.060	0.060
1.000	0.86348	0.00186	0.008	0.01500	0.058	0.058

PTI and CHARA samples (as noted §2). The ratios of the CHARA to PTI UD angular sizes for those four stars (HD3651, HD75732, HD143761, HD217014) are 1.15 ± 0.14 , 1.05 ± 0.10 , 0.99 ± 0.13 , 1.08 ± 0.13 , respectively, with an overall weighted average ratio of 1.06 ± 0.06 , indicating possibly a slight tendency for the PTI sizes to be too small (or the CHARA sizes to be too large), but this is a weak $1\text{-}\sigma$ result.

As a further check on the consistency of the CHARA

results and our techniques, we modeled the predicted SED sizes of the calibrators found in Baines et al. (2008a). These results are seen in Table 3; on average, our calibrator predictions are within 0.5σ , and no individual results are more than 1.9σ away from Baines et al. (2008a). Overall, we find that the CHARA and PTI results are excellent agreement with each other, despite independently developed methodologies.

5. STELLAR PARAMETERS

For both the EHSA and our control sample stars, the basic astrophysical parameters of effective temperature and linear radius are computed from the angular size data and ancillary supporting data. These parameters are then compared between the two samples as a function of $(V - K)_0$ color and, in the case of temperature, spectral type; the results of sections §5.1 and §5.2 are found in Table 4.

5.1. Effective Temperatures

Stellar effective temperature, T_{EFF} , is defined in terms of the star's luminosity and radius by $L = 4\pi\sigma R^2 T_{\text{EFF}}^4$. As noted in §1, rewriting this equation in terms of angular diameter (θ_{LD}) and bolometric flux (F_{BOL}), T_{EFF} can be expressed as $T_{\text{EFF}} = 2341 \times (F_{\text{BOL}}/\theta_{\text{LD}}^2)^{1/4}$, where F_{BOL} is in 10^{-8} ergs cm^{-2} s^{-1} and θ_{LD} is in mas (van Belle et al. 1999). The derived temperature values for the resolved stars of this study are found in Table 4, along with $(V - K)_0$ color. These temperatures are plotted versus $(V - K)_0$ in Figure 1, and to explore any potential difference between the EHSA stars and the control sample, a fit of the T_{EFF} versus $(V - K)_0$ trend is performed.

For the control sample, the initial fit reveals HD87901 as a significant outlier. This is most likely due to two factors: (1) HD87901 is bluest and hottest star, at $(V - K)_0 = -0.352$ and $T_{\text{EFF}} = 14231 \pm 314\text{K}$, and (2) HD87901 is a rapid rotator with $v \sin i = 300$ km/s (Abt et al. 2002), and will show departures from sphericity that induce gravity darkening which render individual T_{EFF} determinations meaningless (Aufdenberg et al. 2006). Omitting HD87901 from the fit, the best fit for the control sample stars is

$$T_{\text{EFF}} = (2832 \pm 239) + (6511 \pm 225) \times 10^{(-0.2204 \pm 0.0255) \times (V - K)_0} \quad (1)$$

with $\chi^2_{\nu} = 1.72$, with the fitting and error ellipses following the techniques described in Press et al. (1992). (Inclusion of HD87901 in this fit returns $\chi^2_{\nu} = 4.98$.)

If we include the EHSA stars in the fit, we find the CHARA data point for 55 Cnc (HD75732) a significant outlier as well, which we will discuss further in §5.4.1. Omitting 55 Cnc from the unified fit, we find a single fit gives:

$$T_{\text{EFF}} = (2974 \pm 199) + (6368 \pm 208) \times 10^{(-0.2362 \pm 0.0227) \times (V - K)_0} \quad (2)$$

with $\chi^2_{\nu} = 1.82$. This fit line is plotted in Figure 1. These fits indicate there is no statistically significant difference between the two populations (noting that the EHSA fit is poorly constrained with a small number of data points over a small range of $(V - K)_0$, preventing a fit to those data alone). We revisit the question of population similarity in further detail in §5.3.

For the fit in Equation 2, the median value of the differences between the T_{EFF} values predicted by this fit and the measured T_{EFF} values is $\overline{\Delta T}_{(V-K)_0} = 138\text{K}$. Since the median value of the errors in the individual T_{EFF} measurements is $\overline{\sigma T} = 164\text{K}$, we believe the limit of precision in the line fit is not due to any intrinsic astrophysical scatter in the T_{EFF} versus $(V - K)_0$ relationship, but rather the limits of the current measurements.

Alternatively, a fit may be made for a cubic relationship between T_{EFF} and $(V - K)_0$, (see, for example, the corresponding equation in Levesque et al. 2005) but this produces no significant improvement:

$$T_{\text{EFF}} = (9455 \pm 313) + (-3590 \pm 483) \times (V - K)_0 + (891 \pm 222) \times (V - K)_0^2 + (-89 \pm 33) \times (V - K)_0^3 \quad (3)$$

with only $\chi^2_{\nu} = 1.68$, in spite of the extra degree of freedom.

For those spectral types for which we have more than one stellar angular size measurement, we can compare the resultant weighted mean T_{EFF} values to the ‘canonical’ values cited in Cox (2000), which can be traced back to the investigation by de Jager & Nieuwenhuijzen (1987). This comparison is seen in Table 5. It is interesting to note that our values of T_{EFF} all track increasingly lower between types F8V to G2V in comparison to the de Jager & Nieuwenhuijzen (1987) values, before returning to agreement with those values at G5V and cooler.

Finally, given the large number of individual samples of our data set between types F6V and G5V, we present an empirical calibration of T_{EFF} versus spectral type for this full range, also in Table 5. Spectral types that have no measurements (e.g., F7V) have T_{EFF} values interpolated from the adjoining spectral types. The average error by spectral type is $\overline{\Delta T}_{\text{SpType}} = 105\text{K}$. This table and Equation 2 represent a direct calibration of the T_{EFF} scale for solar-like main sequence stars for the spectral type range F6V-G5V and color range $(V - K)_0 = 0.0 - 4.0$. No attempt

TABLE 3
COMPARISON OF SPECTRAL ENERGY DISTRIBUTION FITS FOR CALIBRATORS
FROM BAINES ET AL. (2008A) AS DISCUSSED IN §4.4.

Target HD	Calibrator HD	Calibrator Size Est. (mas)	CHARA Est. (mas)	Difference (mas)	σ
3651	4568	0.363 ± 0.008	0.347 ± 0.006	-0.016	1.6
11964	13456	0.407 ± 0.009	0.380 ± 0.011	-0.027	1.9
19994	19411	0.484 ± 0.030	0.485 ± 0.019	0.001	0.0
75732	72779	0.415 ± 0.013	0.413 ± 0.010	-0.002	0.1
143761	136849	0.236 ± 0.035	0.255 ± 0.016	0.019	-0.5
189733	190993	0.166 ± 0.035	0.167 ± 0.035	0.001	0.0
217014	218261	0.387 ± 0.009	0.384 ± 0.015	-0.003	0.2

TABLE 4
DEREDDENED COLORS, EFFECTIVE TEMPERATURES AND RADII FOR LUMINOSITY
CLASS V STARS, DISCUSSED IN §5.

Star ID	$V_0 - K_0$ (mag)	T_{EFF} (K)	d (pc)	R (R_{\odot})
Control Sample: Stars not known to host planets:				
HD1326	4.095 ± 0.053	3584 ± 105	3.568 ± 0.013	0.393 ± 0.023
HD4628	2.125 ± 0.052	4929 ± 169	7.460 ± 0.048	0.749 ± 0.051
HD16160	2.247 ± 0.052	5262 ± 216	7.209 ± 0.054	0.650 ± 0.053
HD16895	1.327 ± 0.091	6200 ± 163	11.232 ± 0.100	1.313 ± 0.069
HD19373	1.395 ± 0.071	5722 ± 110	10.534 ± 0.074	1.509 ± 0.058
HD20630	1.511 ± 0.052	5908 ± 232	9.159 ± 0.065	0.882 ± 0.069
HD22484	1.358 ± 0.101	6618 ± 449	13.719 ± 0.147	1.345 ± 0.183
HD30652	0.925 ± 0.061	7067 ± 124	8.026 ± 0.061	1.217 ± 0.043
HD39587	1.404 ± 0.071	5766 ± 144	8.663 ± 0.081	1.047 ± 0.053
HD87901	-0.352 ± 0.061	14231 ± 314	23.759 ± 0.446	3.092 ± 0.147
HD88230	3.347 ± 0.051	4156 ± 89	4.873 ± 0.019	0.649 ± 0.028
HD95735	4.031 ± 0.051	3593 ± 60	2.548 ± 0.006	0.395 ± 0.013
HD97603	0.106 ± 0.062	8899 ± 201	17.693 ± 0.260	2.281 ± 0.106
HD102647	0.194 ± 0.052	8759 ± 158	11.091 ± 0.109	1.657 ± 0.060
HD109358	1.530 ± 0.072	5896 ± 145	8.371 ± 0.058	1.025 ± 0.050
HD114710	1.311 ± 0.100	6167 ± 165	9.155 ± 0.060	1.056 ± 0.057
HD119850	4.060 ± 0.052	3664 ± 153	5.431 ± 0.037	0.481 ± 0.040
HD126660	1.175 ± 0.073	6358 ± 161	14.571 ± 0.119	1.772 ± 0.087
HD141004	1.423 ± 0.081	6662 ± 477	11.754 ± 0.111	1.060 ± 0.152
HD142860	1.168 ± 0.062	6496 ± 153	11.121 ± 0.089	1.389 ± 0.065
HD149661	1.648 ± 0.052	5196 ± 196	9.778 ± 0.081	0.934 ± 0.070
HD157881	3.419 ± 0.052	4030 ± 242	7.720 ± 0.057	0.564 ± 0.068
HD185144	1.845 ± 0.081	5628 ± 148	5.767 ± 0.015	0.678 ± 0.035
HD201091	2.546 ± 0.051	4526 ± 66	3.482 ± 0.018	0.610 ± 0.018
HD201092	3.431 ± 0.051	4077 ± 59	3.503 ± 0.009	0.628 ± 0.017
HD210027	1.267 ± 0.071	6359 ± 141	11.756 ± 0.098	1.526 ± 0.068
HD215648	1.243 ± 0.082	6461 ± 190	16.250 ± 0.203	1.787 ± 0.106
HD222368	1.245 ± 0.081	6521 ± 179	13.791 ± 0.167	1.577 ± 0.087
EHSA Sample: Known planet hosting stars (PTI):				
HD3651	1.914 ± 0.051	5438 ± 324	11.107 ± 0.089	0.818 ± 0.098
HD9826	1.239 ± 0.081	6465 ± 188	13.468 ± 0.131	1.480 ± 0.087
HD28305	2.168 ± 0.052	4990 ± 50	47.529 ± 1.852	12.692 ± 0.545
HD75732	1.935 ± 0.221	4952 ± 216	12.531 ± 0.132	1.100 ± 0.096
HD95128	1.180 ± 0.341	6140 ± 294	14.077 ± 0.131	1.172 ± 0.111
HD117176	1.625 ± 0.052	5687 ± 188	18.109 ± 0.239	1.858 ± 0.124
HD120136	0.933 ± 0.053	6680 ± 260	15.596 ± 0.170	1.450 ± 0.112
HD143761	1.439 ± 0.052	5936 ± 339	17.428 ± 0.216	1.306 ± 0.149
HD217014	1.432 ± 0.051	5800 ± 338	15.361 ± 0.179	1.141 ± 0.133
EHSA Sample: Known planet hosting stars (CHARA):				
HD3651	1.914 ± 0.051	5062 ± 88	11.107 ± 0.089	0.944 ± 0.033
HD11964	1.543 ± 0.022	5413 ± 359	33.979 ± 1.051	2.234 ± 0.304
HD19994	1.189 ± 0.238	6109 ± 111	22.376 ± 0.376	1.898 ± 0.070
HD75732	1.831 ± 0.042	4836 ± 75	12.531 ± 0.132	1.152 ± 0.035
HD143761	1.439 ± 0.052	5981 ± 194	17.428 ± 0.216	1.287 ± 0.084
HD189733	2.051 ± 0.028	4939 ± 158	19.253 ± 0.322	0.781 ± 0.051
HD217014	1.432 ± 0.051	5571 ± 102	15.361 ± 0.179	1.237 ± 0.047

was made for T_{EFF} calibration for the later types due to the sparseness of the data, although our data at K1V, K7V and M2V represent T_{EFF} calibration for those specific spectral types.

5.2. Linear Radii

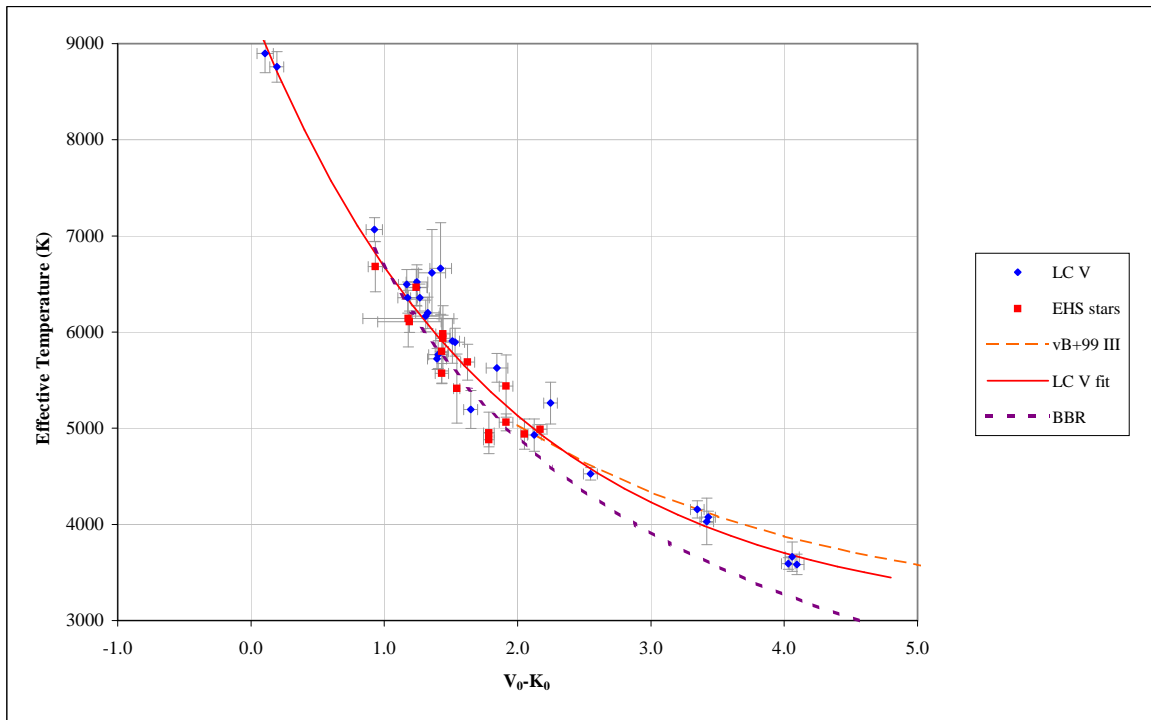


FIG. 1.— Effective temperature T_{EFF} versus $(V - K)_0$ color for control sample and EHS stars. Also shown is a fit to the luminosity class V stars (solid line, discussed in §5.1), the relationship for giants found in van Belle et al. (1999) (dashed line) and for a blackbody radiator (dotted line). The median deviation of the stellar data points from the solid line fit is $\overline{\Delta T} = 138\text{K}$.

From the parallax values found in Table 6 from Hipparcos (Perryman et al. 1997), linear radii are derived for the resolved stars of this investigation and are found in Table 4. A cubic relationship fit to the combined EHS and control samples is:

$$R = (2.263 \pm 0.026) + (-1.261 \pm 0.016) \times (V - K)_0 + (0.347 \pm 0.011) \times (V - K)_0^2 + (-0.036 \pm 0.010) \times (V - K)_0^3 \quad (4)$$

with a $\chi^2_\nu = 15.1$. Clearly this metric indicates a poor fit, which is consistent with some of the stars beginning to evolve well off of the zero-age-main-sequence (ZAMS) line. This effect is seen in a plot of the data in Figure 2, with the presumably older stars being situated to the right of the line fit. As such, Equation 4 should be regarded as only a rough indication of stellar radius, and not applicable in any general sense to determining linear radii of random field stars.

5.3. Kolmogorov-Smirnov Comparison Between Exoplanet Hosting Stars and Control Stars

As detailed in Press et al. (1992), the Kolmogorov-Smirnov (KS) test can be executed to compare two arrays of data values, and examine the probability that the two arrays are drawn from the same distribution. The KS test returns two values: the KS statistic D , which specifies the maximum deviation between the cumulative distribution of the two sample of data, and probability p , giving the significance of the KS statistic. Small values of p (< 0.20) show that the two distributions differ significantly.

Examining the T_{EFF} versus $(V - K)_0$ data of the EHS stars versus the control sample stars, we find that $D = 0.25$ with $p = 0.54$ – strong indication that two data sets are indeed statistically indistinguishable. The astrophysical implication is that, within the limits of our measurements, the effective temperature scale of stars with known planets does not differ from those without known planets.

The corresponding R versus $(V - K)_0$ KS test, how-

ever, reports $D = 0.50$ and $p = 0.01$, which seems to indicate the two samples are inconsistent with each other. However, the significance of this result is simple: our control sample is specifically selected to be main sequence stars, whereas the EHS sample includes a number of evolved sources, as clearly seen in Figure 2. One corollary implication of these two KS tests is that stars on main sequence and those evolving off of it do not differ significantly in their T_{EFF} versus $(V - K)_0$ relationships.

5.4. Comparison with Previous Studies

There is a variety of data available for the known EHSs in the literature, derived from different methods by different authors. Thus, discrepancies, though sometimes small, exist. In order to be as consistent as possible, we chose the following two catalogs as data sources for astrophysical parameters:

- Mass, age, T_{EFF} and $[\text{Fe}/\text{H}]$ from Valenti & Fischer (2005)
- Linear radius from Takeda et al. (2007)

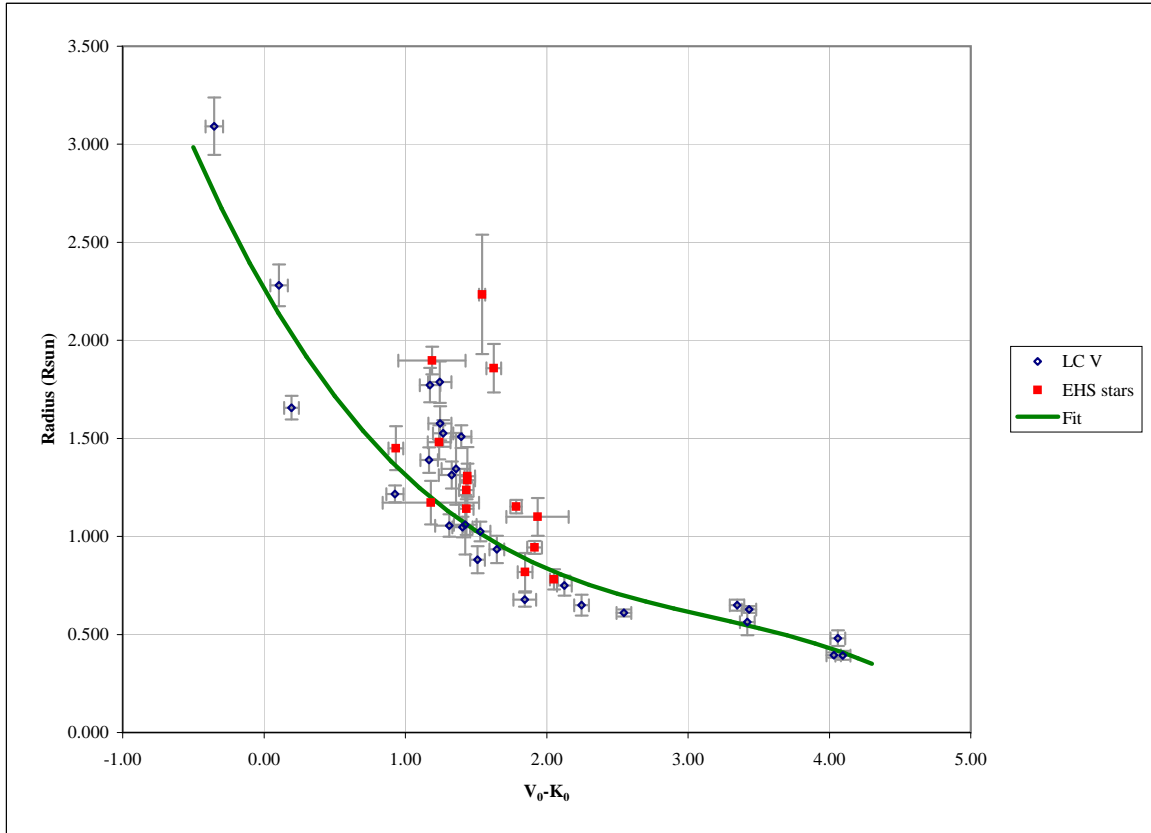


FIG. 2.— Linear radius R versus $(V - K)_0$ color for control sample and EHAS stars as discussed in §5.2. Also shown is a fit to the control sample and EHAS stars (solid line). One of our EHAS stars, HD28305, is a giant star with $\{(V - K)_0 = 2.168 \pm 0.052, R = 12.692 \pm 0.545 R_\odot\}$ and is off the scale of this plot.

TABLE 5
EFFECTIVE TEMPERATURE VERSUS
SPECTRAL TYPE, WITH AN EMPIRICAL
CALIBRATION OF EFFECTIVE
TEMPERATURE VERSUS SPECTRAL TYPE
FOR TYPES F6V THROUGH G5V.

Spectral Type	N	T_{EFF} (K)	$T_{\text{EFF,Cox}}$ (K)
F6V	6	6582 ± 64	6515 ^a
F7V		6394 ± 104	6385 ^a
F8V	4	6206 ± 81	6250
F9V		6025 ± 105	6095 ^a
G0V	7	5844 ± 66	5940
G1V		5717 ± 118	5865 ^a
G2V	2	5590 ± 97	5790
G3V		5562 ± 150	5715 ^a
G4V		5534 ± 150	5635 ^a
G5V	4	5507 ± 115	5560
K1V	4	4966 ± 53	4990 ^a
K7V	3	4099 ± 48	4125 ^a
M2V	3	3599 ± 49	3520

NOTE. — See discussion at end of §5.1. Data after G5V were sufficiently sparse to not merit empirical calibration of the full range. N is the number of angular size measurements per spectral type; rows with no value for N are interpolated values. Columns 3 and 4 are from this work and Cox (2000), respectively.

^a No specific value given in Cox (2000), interpolated from neighboring data points.

A comparison of the T_{EFF} values measured in this investigation can be directly contrasted against those found in Valenti & Fischer (2005). Combining our EHAS and control star samples, we find:

$$T_{\text{EHS}} = (-123 \pm 693) + (1.023 \pm 0.122) \times T_{\text{FV05}} \quad (5)$$

with $\chi_\nu^2 = 1.66$. As illustrated in Figure 3, there is no significant difference between the T_{EFF} values obtained with interferometry and spectroscopy.

A marginal offset is found between our R and the radii of Takeda et al. (2007):

$$R_{\text{EHS}} = (0.071 \pm 0.047) + (0.930 \pm 0.059) \times R_{\text{T+07}} \quad (6)$$

with $\chi_\nu^2 = 1.87$ – roughly a $2\text{-}\sigma$ offset between the line slope and intercept values for R from theory versus those determined interferometrically. The general trend is for the larger ($R > 1.2R_\odot$) stars to have a larger theoretical, rather than interferometric, linear size. These values and the general trend can be seen in Figure 4.

5.4.1. Discussion of 55 Cnc (HD 75732)

Inclusion of the PTI and CHARA data points for 55 Cnc⁶ in the fit of Equation 2 pushes the χ_ν^2 from 1.82

⁶ 55 Cnc’s distance is 12.53 ± 0.13 pc (Perryman et al. 1997). It is KOIV-V star (Gray et al. 2003) with $V = 5.398$ (Bessell 2000). It has a mass of $0.92 \pm 0.046 M_\odot$, an age of $9.5^{+3.4}_{-5.1}$ Gyr, $T_{\text{EFF}} = 5235 \pm 44$ K, and $[\text{Fe}/\text{H}] = 0.31 \pm 0.03$ (Valenti & Fischer 2005). Its radius is $0.91 R_\odot$ in Pasinetti Fracassini et al. (2001) and $1.04 \pm 0.06 R_\odot$ when using the equations in Lang (1980). The values from this investigation are: $T_{\text{EFF}} = 4952 \pm 216$, $R = 1.100 \pm 0.096 R_\odot$.

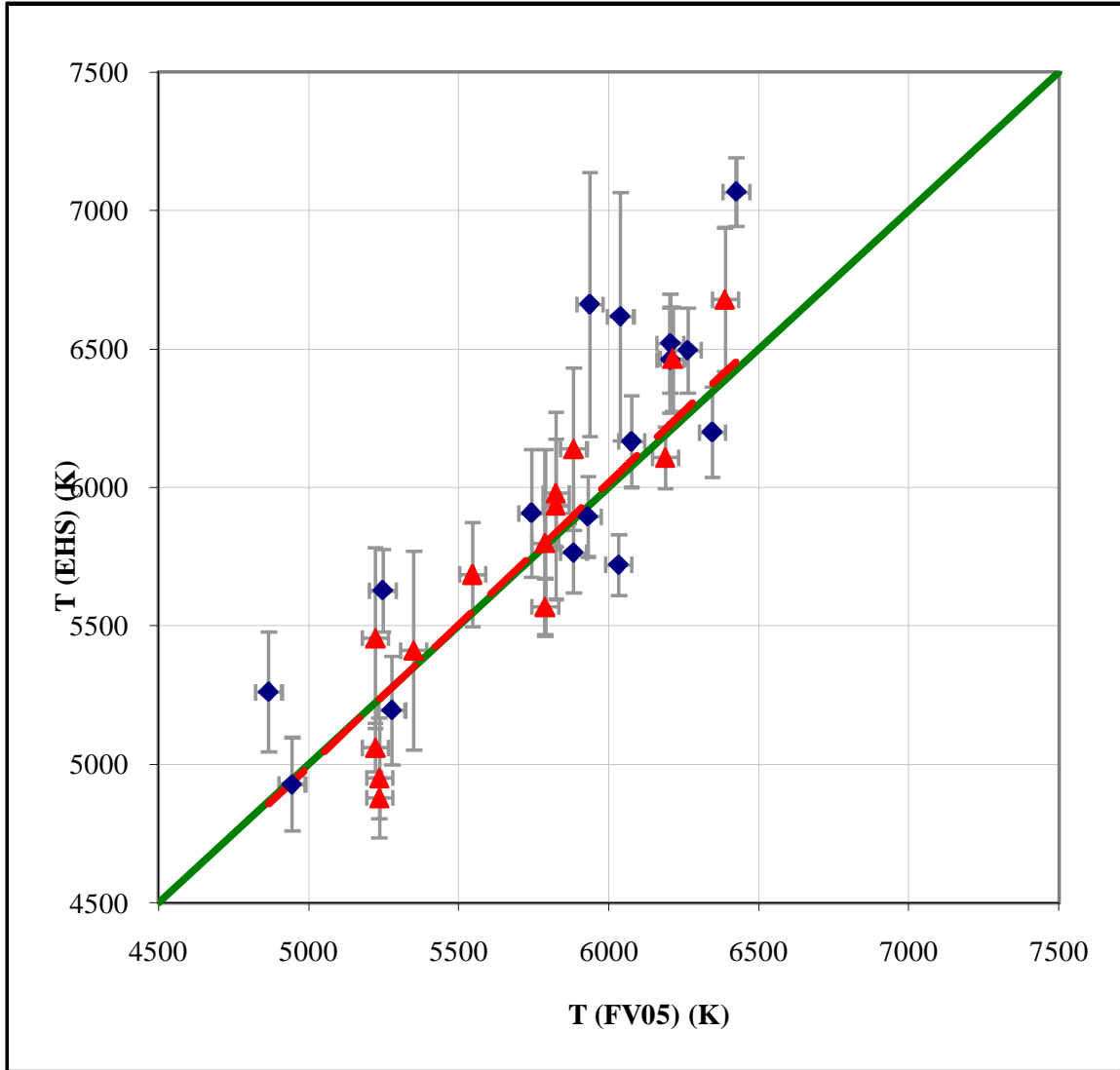


FIG. 3.— Effective temperature as determined by this study, versus those values found spectroscopically by Valenti & Fischer (2005) for EHS stars (red triangles) and our control sample stars (blue diamonds), as discussed in §5.3. The solid line is the 1:1 line, with the dotted line the fit to the T_{EHS} versus T_{VF05} data points.

up to 2.91, with the CHARA data points remaining as $6 - \sigma$ outliers; inclusion of just the PTI points results in $\chi^2_{\nu} = 1.88$. As such, we decided to omit both the CHARA and PTI data points for 55 Cnc from the fit. There are two possible reasons for 55 Cnc turning up as “too cool” to fall onto the T_{EFF} versus $(V - K)_0$ fit of Equation 2.

First, the CHARA data points could be in error: including just the PTI data for 55 Cnc does not significantly alter the resulting χ^2_{ν} value. However, the angular size and T_{EFF} values for 55 Cnc from PTI and CHARA are in direct agreement with each other, although the PTI size data point has a larger error, indicative of its lesser resolving power for this ~ 0.85 mas star. To ‘force’ the 55 Cnc data onto the T_{EFF} versus $(V - K)_0$ fit line, its angular size would need to be reduced to ~ 0.70 mas. Calibrator size error does not appear to be the source of the problem: the size of calibrator HD72779 quoted in Baines et al. (2008a) is $\theta_{\text{EST}} = 0.413 \pm 0.010$ mas – confirmed independently in this investigation with a value of 0.415 ± 0.013 mas – and would have to be ~ 0.65 mas to push the 55 Cnc visibility data to deliver the larger angu-

lar size. Alternatively, the F_{BOL} calculation for 55 Cnc could be too low, but require an increase from 1.4×10^{-8} erg cm $^{-2}$ s $^{-1}$ to $\sim 2 \times 10^{-8}$ erg cm $^{-2}$ s $^{-1}$, which is far outside the allowable bounds of SED fitting, regardless of the template selected.

The second possible reason is that the visibility data could be contaminated by the presence of a secondary stellar companion. Such a companion would reduce the observed visibility, resulting in an apparent increase in angular size, which in turn would effect an apparent decrease in derived temperature - as seen with the 55 Cnc data. Examination of the $\{u, v\}$ plots associated with the CHARA dates and configuration cited in Baines et al. (2008a) indicate a small amount ($< 20^\circ$) of baseline rotation, with nearly zero change in baseline length, which would have lead to a null result in detection in Baines et al. (2008b) for a secondary stellar companion - even in some cases where one is present. There is a known companion to 55 Cnc at a distance of ~ 1000 pc, or $9''.5$ on the sky; however, with $\Delta K = 3.65$ (based on a spectral type of $\sim M4$), in the worst case we would see

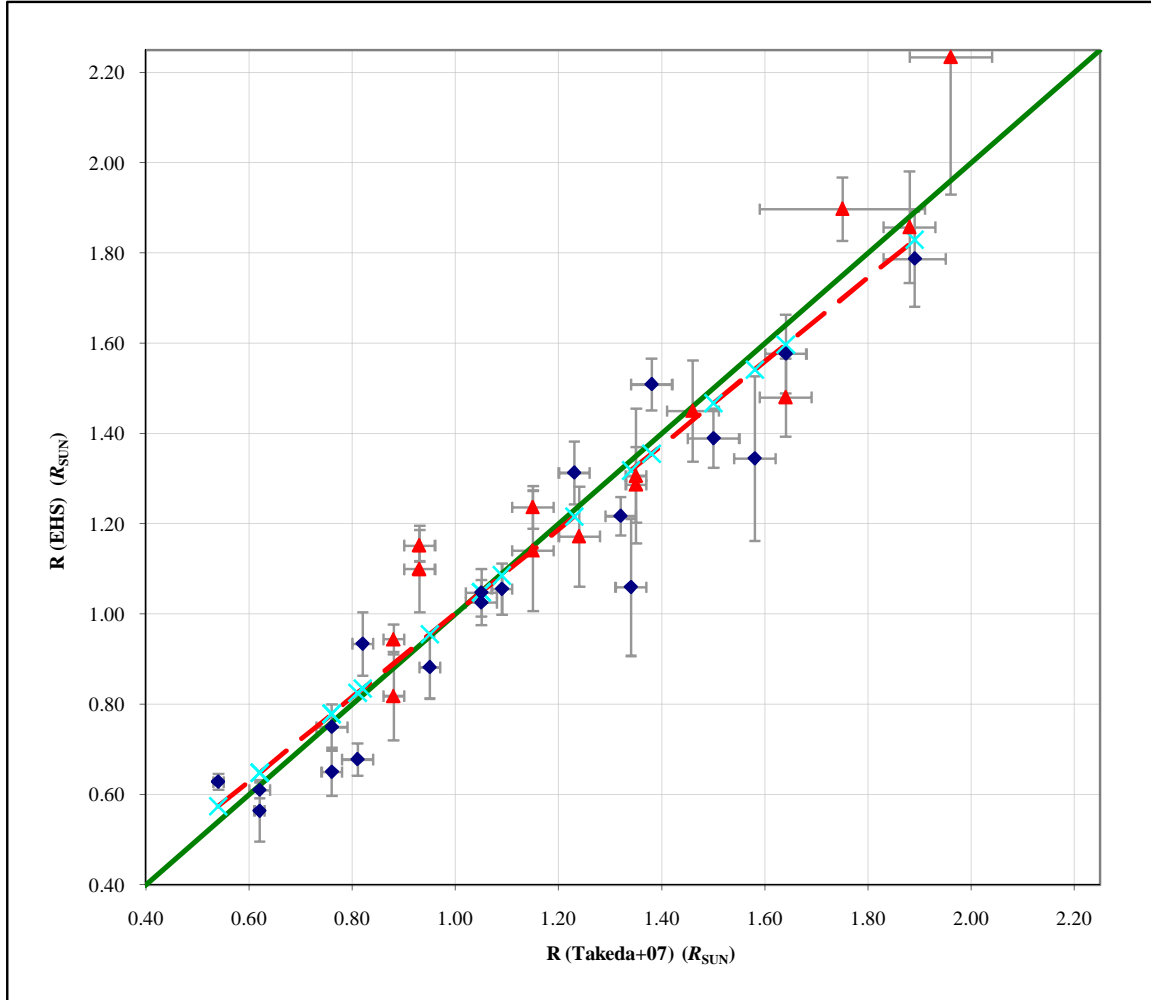


FIG. 4.— Linear radii as determined by this study, versus those values found spectroscopically by Takeda et al. (2007) for EHS stars (red triangles) and our control group (blue diamonds). The solid line is the 1:1 line, with the dotted line the fit to the $R_{\text{EHS}}/R_{\text{Takeda}}$ values. A trend is seen with the larger ($R > 1.2R_{\odot}$) stars being larger in the Takeda et al. (2007) study.

a visibility change of only $\Delta V \sim 0.02$, which would only lower the apparent size from ~ 0.85 to 0.82 mas. Additionally, our naïve expectation is that the intensive spectroscopic studies of 55 Cnc that have turned up no less than 5 planets (Fischer et al. 2008) would have uncovered such a companion, so we are at a loss as to how to reconcile interferometric data with the spectroscopic discoveries. For the moment we will be content to simply remove it from the effective temperature scale calibrations presented in §5.1.

6. SUMMARY AND CONCLUSION

We present directly determined stellar radii and effective temperatures for 12 exoplanet host stars, along with the same estimates for 28 main-sequence control stars not known to host planets. In the process, we demonstrate the empirical limit of PTI’s stellar angular resolution and the implications for angular sizes measured near that limit. While our results show consistency between the direct measurements of effective temperature and indirectly determined literature values, a small difference exists between our radii measurements and theoretical estimates in the sense that for larger stars, the theoretical estimate falls slightly above the direct measurement. From our effective temperature measurements, an empir-

ical calibration of effective temperature versus $(V - K)_0$ color and spectral type is presented, with a spread of $\overline{\Delta T}_{(V-K)_0} = 138\text{K}$ over the range $(V - K)_0 = 0.0 - 4.0$ and $\overline{\Delta T}_{\text{SpType}} = 105\text{K}$ for F6V – G5V. No such calibration is possible for linear radius versus $(V - K)_0$ color, due to the large spread in radius values for any given $(V - K)_0$ color (presumably due to stellar evolution effects). Among the stars considered, 55 Cnc is found to be problematic in terms of its interferometrically determined effective temperature, for reasons that are unclear. Finally, the spectral energy distribution fitting tools employed in this investigation also enable indirect estimates of stellar angular size to be attempted for the full ensemble of stars known to host extrasolar planets, and this database of 166 stars is presented in the “X0-Rad” appendix.

We would like to acknowledge constructive input and the occasional snide comment from David Ciardi. This investigation has made extensive use of the `sedFit` code, graciously provided by `perl` guru Andrew F. Boden. The preparation of this manuscript was greatly helped by the

use of the Extrasolar Planet Encyclopedia⁷. This research made use of the NASA/IPAC/NEExSci Star and Exoplanet Database (NStED)⁸, which is operated by the Jet Propulsion Laboratory, California Institute of Technology, under contract with the National Aeronautics and Space Administration. This publication makes use of data products from the Two Micron All Sky Survey, which is a joint project of the University of Massachusetts and the Infrared Processing and Analysis Center/California Institute of Technology, funded by the Na-

tional Aeronautics and Space Administration and the National Science Foundation. The Palomar Testbed Interferometer is operated by the NASA Exoplanet Science Institute/Michelson Science Center on and the PTI collaboration and was constructed with funds from the Jet Propulsion Laboratory, Caltech as provided by the National Aeronautics and Space Administration. This work has made use of services produced by the NASA Exoplanet Science Institute at the California Institute of Technology.

⁷ Available at <http://exoplanet.eu>.

⁸ Available at <http://nsted.ipac.caltech.edu>.

APPENDIX

THE X0-RAD DATABASE

For the full list of ~ 230 stars found at the Extrasolar Planet Encyclopedia (as of 1 Feb 2008), we collected photometry and performed SED fits as described in the main manuscript in §3, and in detail in van Belle et al. (2008). 64 of the stars have insufficient photometry and were dropped from the SED fitting. The resultant 166 fits provide estimates of bolometric flux F_{BOL} , V-band reddening A_V , angular size θ_{EST} , and linear radius R_{EST} . Effective temperatures are constrained to be those associated with the best fitting Pickles (1998) empirical template. Spectral types used in the SED fitting for EHS stars are those values found in the Exoplanet Encyclopedia, which is in turn based upon the respective source discovery papers cataloged therein. The non-planet-hosting main sequence stars have their spectral types established from those values found in Hipparcos catalog (Perryman et al. 1997). Linear radius is computed by combining the angular size estimates with the Hipparcos data found in van Leeuwen (2007). For a few of the stars, the linear radius is too large to be consistent with the main sequence spectral types indicated in the literature; for these objects, a second iteration on the SED fit is performed with a subgiant (luminosity class IV) template, resulting in a more appropriate set of fit parameters $\{F_{\text{BOL}}, A_V, \theta_{\text{EST}}, R_{\text{EST}}\}$. The full X0-Rad dataset of exoplanet radii is seen in Table 7.

REFERENCES

- Abt, H. A., Levato, H., & Grosso, M. 2002, *ApJ*, 573, 359
- Aufdenberg, J. P., Mérand, A., Coudé du Foresto, V., Absil, O., Di Folco, E., Kervella, P., Ridgway, S. T., Berger, D. H., ten Brummelaar, T. A., McAlister, H. A., Sturmman, J., Sturmman, L., & Turner, N. H. 2006, *ApJ*, 645, 664
- Baines, E. K., McAlister, H. A., ten Brummelaar, T. A., Turner, N. H., Sturmman, J., Sturmman, L., Goldfinger, P. J., & Ridgway, S. T. 2008a, *ApJ*, 680, 728
- Baines, E. K., McAlister, H. A., ten Brummelaar, T. A., Turner, N. H., Sturmman, J., Sturmman, L., & Ridgway, S. T. 2008b, *ApJ*, 682, 577
- Baines, E. K., van Belle, G. T., ten Brummelaar, T. A., McAlister, H. A., Swain, M., Turner, N. H., Sturmman, L., & Sturmman, J. 2007, *ApJ*, 661, L195
- Bessell, M. S. 2000, *PASP*, 112, 961
- Boden, A. F., Colavita, M. M., van Belle, G. T., & Shao, M. 1998, in Presented at the Society of Photo-Optical Instrumentation Engineers (SPIE) Conference, Vol. 3350, Proc. SPIE Vol. 3350, p. 872-880, *Astronomical Interferometry*, Robert D. Reasenberg; Ed., ed. R. D. Reasenberg, 872-880
- Boden, A. F., Koresko, C. D., van Belle, G. T., Colavita, M. M., Dumont, P. J., Gubler, J., Kulkarni, S. R., Lane, B. F., Mobley, D., Shao, M., Wallace, J. K., The PTI Collaboration, & Henry, G. W. 1999, *ApJ*, 515, 356
- Boltzmann, L. 1884, *Annalen der Physik und Chemie*, 22, 291
- Cardelli, J. A., Clayton, G. C., & Mathis, J. S. 1989, *ApJ*, 345, 245
- Colavita, M. M. 1999, *PASP*, 111, 111
- Cox, A. N. 2000, *Allen's astrophysical quantities (Allen's astrophysical quantities, 4th ed. Publisher: New York: AIP Press; Springer, 2000. Edited by Arthur N. Cox. ISBN: 0387987460)*
- Cutri, R. M., Skrutskie, M. F., van Dyk, S., Beichman, C. A., Carpenter, J. M., Chester, T., Cambresy, L., Evans, T., Fowler, J., Gizis, J., Howard, E., Huchra, J., Jarrett, T., Kopan, E. L., Kirkpatrick, J. D., Light, R. M., Marsh, K. A., McCallon, H., Schneider, S., Stiening, R., Sykes, M., Weinberg, M., Wheaton, W. A., Wheelock, S., & Zacharias, N. 2003, *2MASS All Sky Catalog of point sources. (The IRSA 2MASS All-Sky Point Source Catalog, NASA/IPAC Infrared Science Archive. <http://irsa.ipac.caltech.edu/applications/Gator/>)*
- Davis, J., Tango, W. J., & Booth, A. J. 2000, *MNRAS*, 318, 387
- de Jager, C. & Nieuwenhuijzen, H. 1987, *A&A*, 177, 217
- Dyck, H. M., Benson, J. A., van Belle, G. T., & Ridgway, S. T. 1996, *AJ*, 111, 1705
- Dyck, H. M., van Belle, G. T., & Thompson, R. R. 1998, *AJ*, 116, 981
- Eggen, O. J. 1963, *AJ*, 68, 483
- Fischer, D. A., Marcy, G. W., Butler, R. P., Vogt, S. S., Laughlin, G., Henry, G. W., Abouav, D., Peek, K. M. G., Wright, J. T., Johnson, J. A., McCarthy, C., & Isaacson, H. 2008, *ApJ*, 675, 790
- Fukugita, M., Shimasaku, K., & Ichikawa, T. 1995, *PASP*, 107, 945
- Gray, R. O., Corbally, C. J., Garrison, R. F., McFadden, M. T., & Robinson, P. E. 2003, *AJ*, 126, 2048
- Johnson, H. L. *Interstellar Extinction*, ed. B. M. Middlehurst (University of Chicago Press, Chicago, IL USA), 167
- Lang, K. R. 1980, *Astrophysical Formulae (A Compendium for the Physicist and Astrophysicist, XXIX, 783 pp. 46 figs., 69 tabs.. Springer-Verlag Berlin Heidelberg New York. Also Springer Study Edition)*
- Levesque, E. M., Massey, P., Olsen, K. A. G., Plez, B., Josselin, E., Maeder, A., & Meynet, G. 2005, *ApJ*, 628, 973
- Moreno, H. 1971, *A&A*, 12, 442
- Mozurkewich, D., Armstrong, J. T., Hindsley, R. B., Quirrenbach, A., Hummel, C. A., Hutter, D. J., Johnston, K. J., Hajian, A. R., Elias, II, N. M., Buscher, D. F., & Simon, R. S. 2003, *AJ*, 126, 2502

- Mozurkewich, D., Johnston, K. J., Simon, R. S., Bowers, P. F., Gaume, R., Hutter, D. J., Colavita, M. M., Shao, M., & Pan, X. P. 1991, *AJ*, 101, 2207
- Pasinetti Fracassini, L. E., Pastori, L., Covino, S., & Pozzi, A. 2001, *A&A*, 367, 521
- Perryman, M. A. C. & ESA, eds. 1997, *ESA Special Publication*, Vol. 1200, *The HIPPARCOS and TYCHO catalogues*.
Astrometric and photometric star catalogues derived from the ESA HIPPARCOS Space Astrometry Mission
- Perryman, M. A. C., Lindegren, L., Kovalevsky, J., Hoeg, E., Bastian, U., Bernacca, P. L., Cr ez e, M., Donati, F., Grenon, M., van Leeuwen, F., van der Marel, H., Mignard, F., Murray, C. A., Le Poole, R. S., Schrijver, H., Turon, C., Arenou, F., Froeschl e, M., & Petersen, C. S. 1997, *A&A*, 323, L49
- Pickles, A. J. 1998, *PASP*, 110, 863
- Piirola, V. 1976, *Observatory and Astrophysics Laboratory University of Helsinki Report*, 1, 0
- Press, W. H., Teukolsky, S. A., Vetterling, W. T., & Flannery, B. P. 1992, *Numerical recipes in C. The art of scientific computing* (Cambridge: University Press, —c1992, 2nd ed.)
- Rufener, F. 1976, *A&AS*, 26, 275
- Scholz, M. & Takeda, Y. 1987, *A&A*, 186, 200
- Stefan, J. 1879, *Sitzungsberichte der mathematisch-naturwissenschaftlichen Classe der kaiserlichen Akademie der Wissenschaften*, 79, 391
- Takeda, G., Ford, E. B., Sills, A., Rasio, F. A., Fischer, D. A., & Valenti, J. A. 2007, *ApJS*, 168, 297
- ten Brummelaar, T. A., McAlister, H. A., Ridgway, S. T., Bagnuolo, Jr., W. G., Turner, N. H., Sturmman, L., Sturmman, J., Berger, D. H., Ogden, C. E., Cadman, R., Hartkopf, W. I., Hopper, C. H., & Shure, M. A. 2005, *ApJ*, 628, 453
- Tuthill, P. G. 1994, *PhD thesis*, , Univ. of Cambridge, (1994)
- Valenti, J. A. & Fischer, D. A. 2005, *ApJS*, 159, 141
- van Belle, G. T., Lane, B. F., Thompson, R. R., Boden, A. F., Colavita, M. M., Dumont, P. J., Mobley, D. W., Palmer, D., Shao, M., Vasisht, G. X., Wallace, J. K., Creech-Eakman, M. J., Koresko, C. D., Kulkarni, S. R., Pan, X. P., & Gubler, J. 1999, *AJ*, 117, 521
- van Belle, G. T. & van Belle, G. 2005, *PASP*, 117, 1263
- van Belle, G. T., van Belle, G., Creech-Eakman, M. J., Coyne, J., Boden, A. F., Akeson, R. L., Ciardi, D. R., Rykoski, K. M., Thompson, R. R., Lane, B. F., & Collaboration, T. P. 2008, *ApJS*, 176, 276
- van Leeuwen, F. 2007, *A&A*, 474, 653
- Zdanavicius, K., Nikonov, V. B., Sudzius, J., Straizys, V., Sviderskiene, Z., Kalytis, R., Jodinskiene, E., Meistas, E., Kavaliauskaite, G., Jasevicius, V., Kakaras, G., Bartkevicius, A., Gurklyte, A., Bartkus, R., Azusienis, A., Sperauskas, J., Kazlauskas, A., & Zitkevicius, V. 1972, *Vilnius Astronomijos Observatorijos Biuletenis*, 34, 3

TABLE 6
OBSERVED AND DERIVED SUPPORTING PARAMETERS FOR LUMINOSITY CLASS V STARS.

Star ID	$N(V^2)$ Points	θ_{UD} (mas)	χ^2_ν	$\bar{\delta}V^2$	$\theta_{\text{LD}}/\theta_{\text{UD}}$	θ_{LD} (mas)	A_V (mag)	$10^{-8} F_{\text{BOL}}$ erg cm $^{-2}$ s $^{-1}$	Spectral Type	V (mag)	K (mag)
Control Sample: Stars not known to host planets:											
HD1326	216	1.009 ± 0.009	1.02	0.058	1.017	1.027 ± 0.059	0.105 ± 0.019	5.79 ± 0.13	-	8.15 ± 0.05	3.96 ± 0.05
HD4628	98	0.911 ± 0.013	1.18	0.042	1.024	0.933 ± 0.064	0.000 ± 0.015	17.12 ± 0.29	K1V	5.74 ± 0.05	3.61 ± 0.05
HD16160	42	0.820 ± 0.045	0.44	0.055	1.022	0.838 ± 0.069	0.065 ± 0.014	17.93 ± 0.31	K3V	5.83 ± 0.05	3.52 ± 0.05
HD16895	118	1.067 ± 0.016	0.62	0.036	1.018	1.086 ± 0.056	0.000 ± 0.015	58.06 ± 0.99	F8	4.11 ± 0.05	2.78 ± 0.09
HD19373	14	1.304 ± 0.022	2.36	0.052	1.021	1.331 ± 0.050	0.015 ± 0.014	63.24 ± 0.95	F9.5V	4.05 ± 0.05	2.64 ± 0.07
HD20630	2	0.878 ± 0.068	0.00	0.000	1.019	0.895 ± 0.070	0.000 ± 0.015	32.46 ± 0.55	G5V	4.85 ± 0.05	3.34 ± 0.05
HD22484	8	0.897 ± 0.122	0.74	0.064	1.016	0.911 ± 0.123	0.055 ± 0.012	52.99 ± 0.77	F8V	4.30 ± 0.05	2.89 ± 0.10
HD30652	38	1.388 ± 0.024	0.30	0.053	1.015	1.409 ± 0.048	0.225 ± 0.010	164.90 ± 2.51	F6V	3.18 ± 0.05	2.05 ± 0.06
HD39587	84	1.102 ± 0.018	1.26	0.068	1.019	1.124 ± 0.056	0.011 ± 0.014	46.45 ± 0.76	G0IV-V	4.40 ± 0.05	2.99 ± 0.07
HD87901	262	1.192 ± 0.008	1.18	0.049	1.015	1.209 ± 0.053	0.150 ± 0.010	1997.00 ± 26.62	B8IVn	1.40 ± 0.05	1.62 ± 0.06
HD88230	64	1.208 ± 0.013	2.02	0.096	1.025	1.238 ± 0.053	0.000 ± 0.011	15.23 ± 0.06	K8V	6.61 ± 0.05	3.26 ± 0.05
HD95735	80	1.417 ± 0.009	0.00	0.001	1.015	1.439 ± 0.048	0.151 ± 0.011	11.49 ± 0.05	Mb	7.51 ± 0.05	3.34 ± 0.05
HD97603	126	1.180 ± 0.010	0.96	0.046	1.015	1.198 ± 0.053	0.205 ± 0.014	299.60 ± 5.69	A5 IV(n)	2.53 ± 0.05	2.24 ± 0.06
HD102647	66	1.368 ± 0.010	0.51	0.016	1.015	1.388 ± 0.049	0.038 ± 0.015	377.50 ± 6.66	A3Va	2.13 ± 0.05	1.90 ± 0.05
HD109358	166	1.117 ± 0.008	0.66	0.036	1.019	1.138 ± 0.055	0.000 ± 0.015	52.12 ± 0.87	G0V	4.25 ± 0.05	2.72 ± 0.07
HD114710	28	1.052 ± 0.014	0.61	0.037	1.018	1.071 ± 0.057	0.073 ± 0.010	55.28 ± 0.64	G0	4.25 ± 0.05	2.87 ± 0.10
HD119850	142	0.811 ± 0.011	0.99	0.062	1.015	0.823 ± 0.069	0.000 ± 0.014	4.06 ± 0.03	K2	8.50 ± 0.05	4.44 ± 0.05
HD126660	134	1.111 ± 0.014	1.35	0.049	1.017	1.130 ± 0.055	0.109 ± 0.022	69.46 ± 1.99	F8	4.05 ± 0.05	2.78 ± 0.07
HD141004	6	0.824 ± 0.118	0.63	0.024	1.016	0.838 ± 0.120	0.044 ± 0.010	46.01 ± 0.58	G0IV-V	4.42 ± 0.05	2.96 ± 0.08
HD142860	58	1.142 ± 0.009	0.42	0.035	1.017	1.161 ± 0.054	0.053 ± 0.014	79.92 ± 1.37	F5	3.84 ± 0.05	2.62 ± 0.06
HD149661	18	0.868 ± 0.027	1.99	0.095	1.023	0.888 ± 0.066	0.324 ± 0.015	19.12 ± 0.50	K1V	5.77 ± 0.05	3.83 ± 0.05
HD157881	26	0.664 ± 0.036	0.35	0.024	1.023	0.679 ± 0.082	0.000 ± 0.014	4.05 ± 0.06	M1V	7.56 ± 0.05	4.14 ± 0.05
HD185144	6	1.070 ± 0.056	0.59	0.018	1.021	1.092 ± 0.057	0.000 ± 0.013	39.86 ± 0.60	G9V	4.68 ± 0.05	2.83 ± 0.08
HD201091	50	1.588 ± 0.008	0.47	0.037	1.025	1.628 ± 0.046	0.000 ± 0.011	37.01 ± 0.48	K5V	5.23 ± 0.05	2.68 ± 0.05
HD201092	16	1.629 ± 0.033	1.05	0.062	1.023	1.666 ± 0.046	0.232 ± 0.012	25.55 ± 0.47	K7V	5.96 ± 0.05	2.32 ± 0.05
HD210027	172	1.186 ± 0.006	2.44	0.055	1.017	1.206 ± 0.053	0.000 ± 0.011	79.17 ± 1.01	F5	3.77 ± 0.05	2.50 ± 0.07
HD215648	248	1.005 ± 0.006	1.09	0.048	1.017	1.022 ± 0.059	0.101 ± 0.017	60.61 ± 1.35	F5	4.20 ± 0.05	2.87 ± 0.08
HD222368	128	1.046 ± 0.015	0.91	0.065	1.016	1.062 ± 0.057	0.148 ± 0.014	67.94 ± 1.38	F8	4.13 ± 0.05	2.75 ± 0.08
EHSA Sample: Known planet hosting stars (PTI):											
HD3651	222	0.670 ± 0.080	1.03	0.082	1.022	0.685 ± 0.081	0.075 ± 0.015	13.84 ± 0.23	K0V	5.88 ± 0.05	3.97 ± 0.05
HD9826	540	1.004 ± 0.058	0.89	0.035	1.017	1.021 ± 0.059	0.000 ± 0.013	60.68 ± 0.91	G0	4.10 ± 0.05	2.86 ± 0.08
HD28305	32	2.422 ± 0.044	1.30	0.028	1.024	2.481 ± 0.045	0.056 ± 0.014	127.10 ± 2.03	K0III	3.53 ± 0.05	1.31 ± 0.05
HD75732	16	0.796 ± 0.069	0.23	0.018	1.024	0.816 ± 0.071	0.000 ± 0.018	13.32 ± 0.26	K0IV-V	5.95 ± 0.05	4.01 ± 0.22
HD95128	48	0.760 ± 0.072	1.34	0.086	1.018	0.774 ± 0.073	0.123 ± 0.024	28.33 ± 0.92	G0	5.04 ± 0.05	3.75 ± 0.34
HD117176	192	0.934 ± 0.061	1.40	0.058	1.021	0.953 ± 0.062	0.121 ± 0.015	31.64 ± 0.62	G0	4.97 ± 0.05	3.24 ± 0.05
HD120136	264	0.850 ± 0.065	0.98	0.048	1.016	0.864 ± 0.066	0.219 ± 0.018	49.49 ± 1.33	F5	4.49 ± 0.05	3.36 ± 0.05
HD143761	354	0.683 ± 0.078	0.31	0.029	1.019	0.697 ± 0.079	0.096 ± 0.016	20.05 ± 0.41	G0V	5.41 ± 0.05	3.89 ± 0.05
HD217014	454	0.677 ± 0.079	1.28	0.069	1.019	0.690 ± 0.080	0.043 ± 0.009	17.94 ± 0.18	G3V	5.46 ± 0.05	3.99 ± 0.05
EHSA Sample: Known planet hosting stars (CHARA):											
HD3651	-	0.773 ± 0.026	-	-	1.022	0.790 ± 0.027	0.000 ± 0.012	13.64 ± 0.18	K0V	5.88 ± 0.05	3.97 ± 0.05
HD11964	-	0.597 ± 0.078	-	-	1.023	0.611 ± 0.081	0.437 ± 0.010	10.67 ± 0.14	G5	6.42 ± 0.05	4.49 ± 0.02
HD19994	-	0.774 ± 0.026	-	-	1.018	0.788 ± 0.026	0.160 ± 0.027	28.79 ± 0.83	F8V	5.08 ± 0.05	3.75 ± 0.24
HD75732	-	0.834 ± 0.024	-	-	1.024	0.854 ± 0.024	0.111 ± 0.022	13.28 ± 0.34	G8V	5.95 ± 0.05	4.02 ± 0.04
HD143761	-	0.673 ± 0.043	-	-	1.019	0.686 ± 0.044	0.096 ± 0.016	20.05 ± 0.41	G0V	5.41 ± 0.05	3.89 ± 0.05
HD189733	-	0.366 ± 0.024	-	-	1.030	0.377 ± 0.024	0.101 ± 0.018	2.82 ± 0.04	K1V	7.68 ± 0.05	5.54 ± 0.02
HD217014	-	0.733 ± 0.026	-	-	1.020	0.748 ± 0.027	0.043 ± 0.009	17.94 ± 0.18	G3V	5.46 ± 0.05	3.99 ± 0.05

TABLE 7 — *Continued*

HD Number	Template	Template T_{EFF} (K)	χ^2_{ν}	N_{PHOT}	F_{BOL} (10^{-8} cm $^{-2}$ s $^{-1}$)	A_V (mag)	θ_{EST} (mas)	R_{EST} (R_{\odot})
202206	G5V	5585 ± 50	1.23	30	1.66 ± 0.01	0.03 ± 0.01	0.226 ± 0.004	1.10 ± 0.05
208487	G2V	5807 ± 50	0.74	22	2.63 ± 0.02	0.00 ± 0.02	0.244 ± 0.004	1.20 ± 0.04
209458	G0V	6040 ± 50	0.14	24	2.37 ± 0.03	0.03 ± 0.02	0.231 ± 0.004	1.23 ± 0.05
210277	G0V	5807 ± 50	2.33	36	9.55 ± 0.15	0.55 ± 0.01	0.502 ± 0.010	1.16 ± 0.03
210702	K1III	4853 ± 130	1.12	63	14.27 ± 0.43	0.01 ± 0.03	0.879 ± 0.049	5.20 ± 0.31
212301	F8V	6280 ± 70	0.15	24	2.29 ± 0.02	0.15 ± 0.01	0.210 ± 0.005	1.24 ± 0.05
213240	F8IV	6152 ± 100	1.03	38	5.33 ± 0.04	0.11 ± 0.01	0.334 ± 0.011	1.46 ± 0.06
216435	G0IV	5929 ± 90	0.38	61	9.90 ± 0.11	0.00 ± 0.01	0.490 ± 0.015	1.72 ± 0.06
216437	G0IV	5929 ± 90	0.93	74	10.52 ± 0.19	0.10 ± 0.02	0.506 ± 0.016	1.46 ± 0.05
216770	G8V	5333 ± 50	2.18	32	1.69 ± 0.01	0.10 ± 0.01	0.250 ± 0.005	0.96 ± 0.03
217014	G2V	5636 ± 50	1.86	214	17.94 ± 0.18	0.04 ± 0.01	0.731 ± 0.014	1.23 ± 0.02
217107	G8IV	5598 ± 80	0.43	43	9.32 ± 0.12	0.01 ± 0.01	0.534 ± 0.016	1.14 ± 0.03
219449	K0III	4853 ± 130	3.71	90	94.46 ± 2.90	0.45 ± 0.02	2.260 ± 0.126	11.17 ± 0.64
219828	G0IV	5929 ± 90	2.47	23	1.70 ± 0.01	0.08 ± 0.01	0.203 ± 0.006	1.58 ± 0.10
221287	F6V	6280 ± 70	0.04	27	2.07 ± 0.02	0.07 ± 0.01	0.200 ± 0.005	1.19 ± 0.05
222582	G5V	5636 ± 50	0.17	30	2.62 ± 0.03	0.18 ± 0.01	0.263 ± 0.005	1.18 ± 0.04
224693	G0IV	5929 ± 90	1.42	23	1.31 ± 0.01	0.01 ± 0.01	0.178 ± 0.006	1.89 ± 0.18
231701	F5IV	6562 ± 150	0.37	15	0.86 ± 0.01	0.31 ± 0.02	0.118 ± 0.005	1.50 ± 0.20

NOTE. — N_{PHOT} is the number of photometric data points available in the literature used for the spectral template fitting described in §3.